IEEE Photonics Journal
An IEEE Photonics Society Publication

Propagation, Resonance, and Radiation on Terahertz Optoelectronic Integrated Circuits

Volume 4, Number 3, June 2012

Yu-Ru Huang
Hung-Pin Chen
Pei-Chin Chiu
Jen-Inn Chyi, Fellow, IEEE
Bing-Hsiao Wang
Shih-Yuan Chen, Senior Member, IEEE
Chi-Kuang Sun, Fellow, IEEE

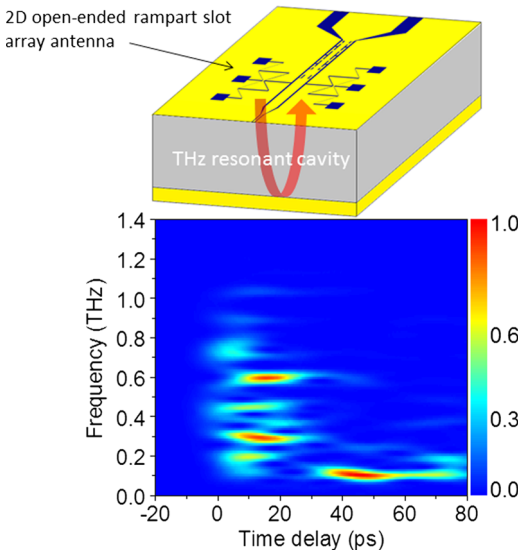

DOI: 10.1109/JPHOT.2012.2195484
1943-0655/$31.00 ©2012 IEEE

IEEE photonics SOCIETY

IEEE

Propagation, Resonance, and Radiation on Terahertz Optoelectronic Integrated Circuits

Yu-Ru Huang,[1] Hung-Pin Chen,[1] Pei-Chin Chiu,[2] Jen-Inn Chyi,[2] *Fellow, IEEE*, Bing-Hsiao Wang,[3] Shih-Yuan Chen,[3] *Senior Member, IEEE*, and Chi-Kuang Sun,[1,4,5] *Fellow, IEEE*

[1]Department of Electrical Engineering and Graduate Institute of Photonics and Optoelectronics, National Taiwan University, Taipei 10617, Taiwan
[2]Department of Electrical Engineering, National Central University, Jhongli 32054, Taiwan
[3]Department of Electrical Engineering and Graduate Institute of Communication Engineering, National Taiwan University, Taipei 10617, Taiwan
[4]Institute of Physics and Research Center for Applied Sciences, Academia Sinica, Taipei 11529, Taiwan
[5]Molecular Imaging Center and Graduate Institute of Biomedical Electronics and Bioinformatics, National Taiwan University, Taipei 10617, Taiwan

DOI: 10.1109/JPHOT.2012.2195484
1943-0655/$31.00 ©2012 IEEE

Manuscript received March 26, 2012; revised April 9, 2012; accepted April 11, 2012. Date of publication April 19, 2012; date of current version May 2, 2012. This work was supported by the National Science Council of Republic of China under Grant NSC100-2120-M-002-009 and Grant NSC100-2221-E-002-183-MY3. Corresponding author: C.-K. Sun (e-mail: sun@cc.ee.ntu.edu.tw).

Abstract: This paper investigates terahertz (THz) wave propagation, resonance, and radiation on a THz optoelectronic integrated circuit (THz-OEIC). An efficient THz resonant radiation from 0.6 to 0.7 THz can be achieved with a newly designed 2-D open-ended rampart slot array antenna. A monolithically integrated circuit is fabricated on a localized THz resonant cavity, which not only provides a robust base for postdevice processes but also helps collect and reradiate the fleeing surface waves to enhance radiation efficiency. When using a THz time-domain spectroscopy (THz-TDS) technique and a time-frequency analysis, the radiated THz waveform shows a good time-frequency correlation to the circuit design of our THz-OEIC. In addition, an optical-to-THz per-pulse conversion efficiency of 6.41×10^{-3} can be achieved by a localized THz resonant cavity design. The enhanced optical-to-THz per-pulse conversion efficiency and THz propagation, resonance, and radiation behavior revealed not only help to understand the on-chip THz transmission phenomena but provide a good potentiality for a THz-OEIC design to be applied in low power-consuming microfluidic-channel-based THz biosensing chips as well.

Index Terms: Terahertz optoelectronic integrated circuits, rampart slot array antenna, THz resonant cavity.

1. Introduction

In order to bridge the terahertz (THz) gap between microwave and far-infrared regimes, various kinds of THz devices have been vigorously developed in the past two decades. These include high-power continuous-wave THz quantum cascade lasers (THz-QCLs) [1], broadband single-cycle THz photoconductive (PC) antennas [2], high-output-power uni-traveling-carrier photodiodes at the sub-THz regime [3], InP-based double-heterojunction bipolar transistors [4], hot electron mobility transistors [5], [6], and record-high power-conversion-efficiency THz photonic transmitters [7]–[9]. Thanks to well-developed THz sources, a wide range of applications have also been successfully demonstrated, including microchip-based biodetection [10], [11], and THz bioimaging [12]–[15].

However, the "on-chip" propagation of the THz waves has rarely been investigated due to the lack of precise THz measuring systems. In the past few years, although the THz wave propagation on passive devices, such as metal plate waveguides [16], [17], had been extensively explored by using a THz time-domain spectroscopy (THz-TDS), the THz transmission phenomenon on a sophisticated active THz-integrated circuit has seldom been revealed. The localized propagation or resonance of THz waves should be carefully considered when designing THz optoelectronic integrated circuits (THz-OEICs), especially for lab-on-a-chip devices in which a microfluidic channel will be integrated, since the constantly applied fluid background is also able to alter the circuit parameters, e.g., the effective permittivity. It is well known that the transmission and reflection of millimeter waves (MMW) on an all-solid-state electronic circuit can be precisely extracted by analyzing the scattering parameters and far field radiations with a vector network analyzer (VNA). Nevertheless, a VNA operated at the THz regime remains unpopular due to the high cost of the whole apparatus, including oscillators, multipliers, transmission lines, antennas, etc. Therefore, studies on the THz wave propagation on an active device are still very scarce. Here, we have designed a THz-OEIC in which a highly efficient edge-coupled metal–semiconductor–metal travelling-wave photodetector (MSM-TWPD), a localized THz resonant cavity, a high-gain 2-D open-ended rampart slot array antenna, a miniature THz electromagnetic band-gap (EBG) low-pass filter, and a direct current (DC) probe pad are monolithically integrated. By utilizing a conventional THz-TDS measuring technique and a time-frequency analysis, the experimentally measured THz radiation shows an excellent time-frequency correlation to our circuit design. In addition, we have successfully attained an enhanced optical-to-THz per-pulse conversion efficiency of 6.41×10^{-3} for the THz-OEIC with a localized THz resonant cavity design. Consequently, our demonstrated THz-OEIC is able to serve as a compact and efficient subsystem to be integrated in more sophisticated THz-OEICs, such as a low-power/high efficiency microfluidic-channel-based on-chip biosensing device.

2. Device Design

2.1. MSM-TWPD and EBG Low-Pass Filter

As an efficient optical-to-electrical converter, a low-temperature-grown gallium arsenide (LTG-GaAs)-based MSM-TWPD has been demonstrated to possess both an ultrawide 3 dB electrical bandwidth of 570 GHz [18] and a record high power-bandwidth product of 5.7 THz-V [19]. Based on a quasi-TEM coplanar waveguide (CPW) mode, the MSM-TWPD preserves a great deal of superior microwave properties, such as a high microwave velocity, lower loss of high-frequency microwaves, and better impedance matching between external loads and the TWPD [20]. Benefiting from a travelling-wave design, the MSM-TWPD is one of the optoelectronic devices which can be easily integrated into monolithic circuits. The THz EBG low-pass filter is designed based on periodic CPW structures [21]. Thanks to the slow-wave effect by applying additional capacitances and inductances into the signal conductor, a miniaturized low-loss CPW-fed THz EBG low-pass filter can be easily fabricated and integrated into our current THz-OEIC circuit. A detailed geometrical design of the low-pass filter can be found in our previous work [9], and the cutoff frequency is designated at 500 GHz in order to reflect high-frequency signals back to the antenna to enhance the radiation efficiency.

2.2. Localized Resonant Cavity and Open-Ended Rampart Slot Array Antenna

In the past few years, a membrane-type THz photonic transmitter has been demonstrated to possess wide frequency tunability, high radiation directivity, and high optical-to-THz power conversion efficiency [8], [9]. However, membrane-type circuits (with a thin substrate thickness of $\sim 5\ \mu$m) are fragile for postdevice processes, e.g., the bonding process with microfluidic-channel chips. Thus, there is a need for a THz-integrated circuit on a robust substrate. On the other hand, it is well known that electromagnetic (EM) waves tend to penetrate into materials with higher dielectric constants. Consequently, the total internal reflection retains the THz waves inside the

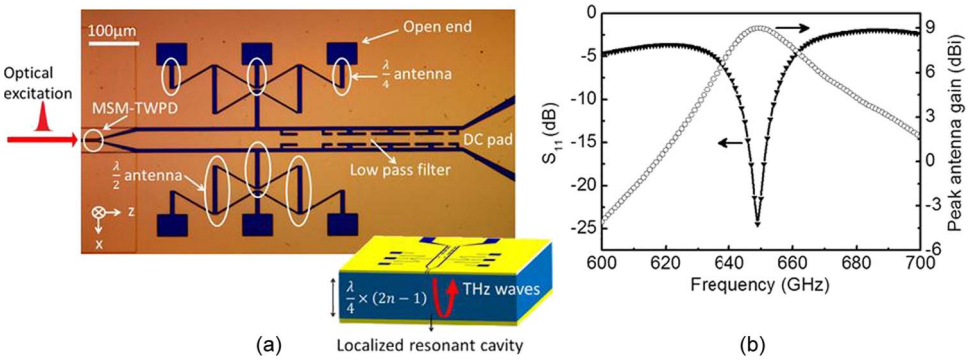

Fig. 1. (a) A microphotograph of our developed THz OEIC, in which a MSM-TWPD, a 2-D folded open-ended rampart slot array antenna, a THz resonant cavity, an EBG low-pass filter, and a DC pad are monolithically integrated. The inset shows the figure of the localized THz resonant cavity design. (b) The calculated return (solid reverse triangle line) and peak antenna gain (hollow circle line) of our proposed THz OEIC.

device substrate to suffer high dielectric loss. To avoid energy dissipation of the excited THz waves in the substrate, we have designed a localized THz resonator under our THz printed circuit based on the design of a grounded CPW (GCPW) structure. As shown in the inset of Fig. 1(a), a thick GaAs substrate with the THz printed circuit developed on top was reserved and a 300-nm thick gold layer was coated onto the bottom of the substrate to reflect the THz waves back to the antenna. A localized THz resonant cavity was thus formed between the THz printed circuit and the high-reflecting gold layer. With a cavity length equivalent to odd multiples of a quarter wavelength, our THz printed circuits can achieve an in-phase oscillation of the THz waves in the localized THz resonant cavity. In view of the requirement for both in-phase oscillations and robust bases, we adopted a substrate thickness of $\sim$132 μm, three-quarter wavelengths.

A 2-D open-ended rampart slot array antenna was adopted to achieve both high THz radiation efficiency and directivity. As shown in Fig. 1(a), each slotline is designated as a half guiding wavelength, except for the outermost quarter-wavelength segments terminated by open circuits. The vertical slotlines, parallel to the *x*-axis, serve as the main radiating elements, while the others are feeding lines. It is known that the guided EM waves tend to flee away in the form of surface waves on a thick dielectric substrate. Instead of utilizing the traditional perpendicular connecting networks, we propose to utilize folded feeding networks. The newly designed rampart slot antenna contains four equilateral triangles to form connecting networks. As before, the vertical segments serve as the main radiating elements. When the THz wave spreads along the two waist slotlines, it generates both horizontal and vertical wave components. The vertical components, parallel to the main radiating elements, can also help to enhance an effective resonance for far-field radiation. In other words, our newly proposed feeding networks can save more surface waves as effective resonances for THz radiation, rather than merely fleeing waves. More design principles of the 2-D open-ended rampart slot array antenna can be found in [22] and [23]. Here, we have adopted a 2-D array with 12 radiating elements as efficient and high-directivity THz radiators.

2.3. THz-OEICs

A microphotographic view of our developed THz-integrated circuit is shown in Fig. 1(a). With the aid of a full-wave 3-D simulation tool, known as IE3D, we carefully optimized the geometry of the entire circuit to achieve a good impedance matching point at 650 GHz. The simulated performance of the entire device is shown in Fig. 1(b). A theoretical peak antenna gain of $\sim$9 dBi could be achieved in our newly designed THz-integrated circuits due to the localized THz resonant cavity design. As for frequencies with a theoretical peak antenna gain below 0 dBi, the THz waves will theoretically propagate on our THz-integrated circuit rather than being radiated.

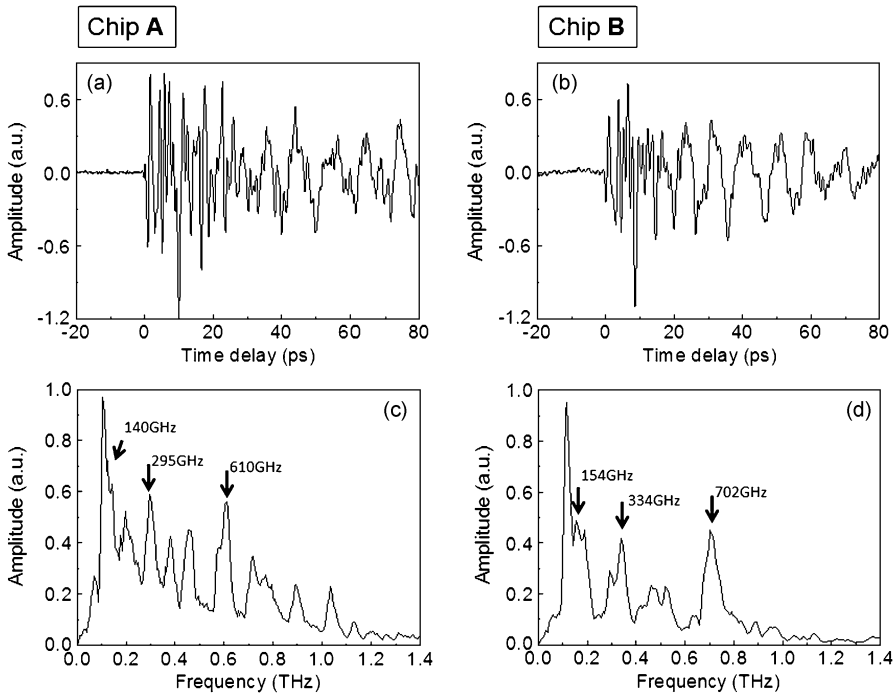

Fig. 2. Measured THz waveforms radiated from chip **A** (a) and chip **B** (b). The spectra of the THz radiations from chip **A** (c) and chip **A** (d). The arrows show the impedance matching frequency at ~650 GHz and its integer multiples of $\lambda_{res}/2$ resonances.

3. Experimental Results and Discussions

To investigate the THz radiation from our OEICs, we used a THz-TDS technique to measure the THz waveform radiating from our chip. A 100-fs Ti:Sapphire laser pulse train with a central wavelength of 800nm and a repetition rate of 80 MHz was edge-coupled into the MSM-TWPD as illustrated in Fig. 1(a). A broadband THz current was on-chip generated from the MSM-TWPD and then conducted toward the 2-D open-ended rampart slot array antenna for radiation. The radiated THz waves were then collected by two off-axis parabolic mirrors and focused into a 2-mm ZnTe electrooptical (EO) crystal. By delaying a probe laser pulse on ZnTe, the waveform of the radiated THz pulse could be measured via the EO sampling technique [24]. The THz radiations from two different chips, one of which was from a chip with a localized THz resonant cavity, denoted as chip **A**, while the other was without the high-reflecting gold layer under the GaAs substrate, denoted as chip **B**, were measured. As shown in Fig. 2, under a 7-V DC bias and an average optical excitation power of 1.32 mW (corresponding to 16.5 pJ/pulse), the radiated THz pulses from both chips were in a chirped form and gave high-frequency components mainly from 0 to ~20 ps. The time zero is defined as the arising point of measured THz radiations. After a time delay of ~20 ps, the low-frequency signals at around 100GHz began to radiate. The corresponding THz wave spectra were easily obtained by Fourier transforming the measured THz waveforms. For the THz spectra, a strong resonance at ~0.6 THz for chip **A** and at ~0.7 THz for chip **B** could be clearly observed, which were close to our designed impedance matching point of 650 GHz. The shift of the peak resonant frequency between these two chips is due to the variation of the effective dielectric constant of the THz propagating modes. Since chip **B** had no grounded gold reflecting layer, the THz fields were not only distributed in the substrate but extended into the free space under the substrate as well, which thus resulted in a lower effective dielectric constant and a higher resonant frequency [25]. It is also worth noting that the measured THz radiation from chip **A** contained more high-frequency components than chip **B**. As already mentioned, the propagating THz surface waves could easily penetrate into the substrate and dissipate. Our current results

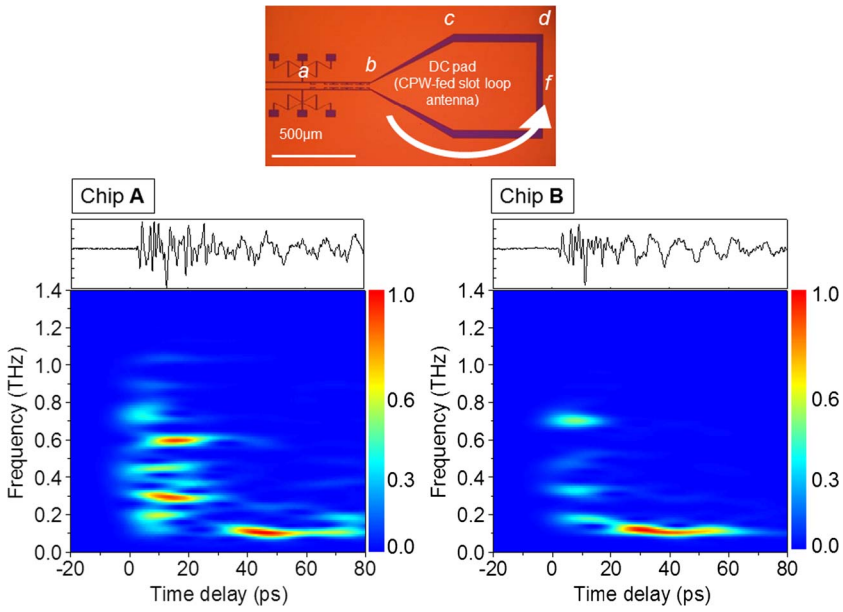

Fig. 3. Time-frequency analysis of the THz waves radiated from THz integrated chip **A** and **B**. The THz waveforms are plotted for correspondence. The high-frequency signals were radiated during 0 to 20 ps by 2-D open-ended rampart slot array antenna while low-frequency signals at ∼100 GHz were radiated after 20 ps by the DC pad. The inset shows the microphotographic view of DC pad, which serves as an efficient CPW-fed slot loop antenna.

confirm that more high-frequency waves can be conserved and reradiated from the chip with the localized THz resonant cavity design. The measured highest frequency component for chip **A** was up to ∼1.1 THz, which agrees quite well with our previously demonstrated frequency tunable range [8] and indicates a possibility to extend our current work toward the frequency range higher than 1 THz.

A *Time-Frequency analysis* [26] was applied to explore the THz wave propagation behavior on our THz-integrated circuits. The time-dependent THz spectrum was plotted as shown in Fig 3. According to the time delay, all the high-frequency signals were mainly radiated during the same period, 0 to ∼20 ps, by the 2-D open-ended rampart slot array antenna. In addition to the main resonant radiation at ∼0.6 to 0.7 THz, it is well known that the resonance of integer multiples of $\lambda_{res}/2$ is also able to take place through the connecting slotlines [27]. As shown in Figs. 2(d) and 3, two resonant peaks at ∼334 and ∼154 GHz could be clearly observed for chip **B** in addition to the original impedance matching frequency of 702 GHz. Similarly, two integer multiples of half-wavelength resonances could be observed for chip **A** as shown in Figs. 2(c) and 3. It should be noted that the observed lower resonant frequencies were slightly red-shifted compared to the expected quarter- and half-frequency resonances. Since the terminating open circuits at the end of antennas were optimized for 650 GHz, it was easy for low-frequency waves to leak into the aperture of the open circuits. The imperfect open circuits for low-frequency waves thus led to resonances at slightly lower frequencies or longer wavelengths, which appeared as our measured red-shifted lower frequency peaks. After being spread through an EBG low-pass filter, the low-frequency components arrived at the DC pad. Since the DC pad could also serve as an efficient CPW-fed slot loop antenna [28], the low-frequency waves at around 100 GHz with a 2.5 $\lambda_{100\ GHz}$ resonance could thus be efficiently radiated by our designed DC pad (as shown in the inset of Fig. 3). In addition, a time delay of more than 20 ps is needed for low-frequency waves to propagate from the input end of the 2-D open-ended rampart slot antenna (point *a* in the inset of Fig. 3) to the radiating element of DC pad (through points *b*, *c*, *d* to *f* as shown in the inset of Fig. 3). It is thus confirmed that the measured waves of ∼100 GHz, as shown in Fig. 3 to appear only after > 20 ps, were radiated by our designed DC pad, which behaved as a CPW-fed slot loop antenna. In short,

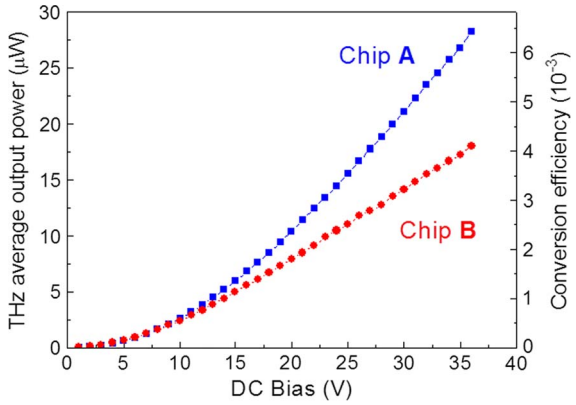

Fig. 4. Measured bias-dependent THz average output power under an average optical excitation power of 4.4 mW. The THz pulse energy could be obtained by dividing the received THz average power by the repetition rate of THz pulses, which was 80 MHz. An enhanced optical-to-THz per-pulse conversion efficiency of 6.41×10^{-3} was achieved by using the design of a localized THz resonator.

the observed THz radiations shows an excellent time-frequency correlation to our circuit design, and the time-frequency analysis can thus help the future design of a more sophisticated THz-OEIC in which phase information is highly required.

The average power of the radiated THz pulses was measured by a liquid-helium-cooled Si bolometer (Infrared Lab., Inc.). As confirmed by the EO sampling measurements, the excited THz pulses were with a waveform as shown in Fig. 2 and with a pulsewidth much shorter than the interval between adjacent optical excitation pulses (12.5 ns). We thus confirmed that the THz pulse radiation was with the same repetition rate as the optical excitation pulses, which was 80 MHz. The THz power measurement setup was kept the same as the EO sampling except the ZnTe crystal and probe laser pulses were replaced by the liquid-helium-cooled Si bolometer. The frequency response of our Si bolometer system was operated in the range of 150 to 3000 GHz. We inserted an optical chopper in the optical path of pump pulses and measured the output of the bolometer with a lock-in amplifier. The responsivity of the Si bolometer was calibrated by using the same method as reported before [7]. It is worth noting that since the frequency responsivity of our Si bolometer system has already filtered out THz signals below 150 GHz, the received THz power is mainly distributed in the frequency range from 0.15 to 1.1 THz with signals at $\sim$100 GHz excluded. The bias-dependent THz power of both chips under a fixed average optical excitation power of 4.4 mW (55 pJ/pulse) was measured. As shown in Fig. 4, a maximum THz average output power of 28.2 and 18.0 μW (corresponding to 0.35 and 0.23 pJ/pulse) could be achieved at a DC bias of 36 V for chips **A** and **B**, respectively. The maximum DC bias of 36 V was limited by the power supply (Agilent Tech., Inc. E3647A). The corresponding external (including coupling and collection loss) per-pulse conversion efficiency was 6.41×10^{-3} (0.35 pJ/55 pJ) and 4.09×10^{-3} (0.23 pJ/55 pJ) for chips **A** and **B**, respectively. Comparing the results from chips **A** and **B**, the measured THz output power confirmed that more THz waves could be received due to the reradiation of THz waves resonating in the localized THz resonant cavity, contributing to an enhanced optical-to-THz per-pulse conversion efficiency. It should be noted that no saturation behavior was observed in our current devices in which the electrode gap in MSM-TWPD was $\sim$1 μm. It is known that THz output power will saturate under a high applied bias voltage due to the Coulomb barrier lowering effect, which will take place over 60-V bias voltage for our current devices [29]–[31]. On the other hand, the applied field in the MSM-TWPD is estimated as 3.6×10^{-5} V/cm, which is still less than the breakdown field of LTG-GaAs of $\sim 5 \times 10^{-5}$ V/cm [32]. Therefore, the maximum THz output power available will be limited by the breakdown voltage, and an even higher optical-to-THz per-pulse conversion efficiency of our device can be expected under a DC bias voltage of more than 50 V.

5. Conclusion

This paper has demonstrated a sophisticated THz-OEIC in which a MSM-TWPD, a 2-D open-ended rampart slot array antenna, a THz EBG low-pass filter, a localized THz resonant cavity, and a DC probe pad were monolithically integrated. An efficient THz radiation at around 0.6 to 0.7 THz can be easily achieved from our newly designed 2-D open-ended rampart slot array antenna. The localized THz resonant cavity not only helps to conserve and reradiate the fleeing waves but provides a robust base for postdevice processes as well. An external optical-to-THz per-pulse conversion efficiency of 6.41×10^{-3} was successfully attained with the localized THz resonant cavity design. In addition, the on-chip propagation of the THz waves on an active THz optoelectronic circuit was investigated for the first time. The good agreement between the time-frequency analysis and the circuit design signifies a great potential of the adopted method for further application design, such as low power-consuming microfluidic-channel-based biosensing THz microchips.

References

[1] S. Kumar, C. W. I. Chan, Q. Hu, and J. L. Reno, "A 1.8-THz quantum cascade laser operating significantly above the temperature of $\hbar\omega/k_B$," *Nature Phys.*, vol. 7, no. 2, pp. 166–171, Feb. 2011.

[2] Z. D. Taylor, E. R. Brown, J. E. Bjarnason, M. P. Hanson, and A. C. Gossard, "Resonant-optical-cavity photoconductive switch with 0.5% conversion efficiency and 1.0 W peak power," *Opt. Lett.*, vol. 31, no. 11, pp. 1729–1731, Jun. 2006.

[3] H. Ito, S. Kodama, Y. Muramoto, T. Furuta, T. Nagatsuma, and T. Ishibashi, "High-speed and high-output InP-InGaAs unitraveling-carrier photodiodes," *IEEE J. Sel. Topics Quantum Electron.*, vol. 10, no. 4, pp. 709–727, Jul./Aug. 2004.

[4] J. Hacker, M. Seo, A. C. Young, Z. Griffith, M. Urteaga, T. Reed, and M. Rodwell, "THz MMICs based on InP HBT technology," in *Proc. IEEE MTT*, 2010, pp. 1126–1129.

[5] V. Radisic, X. B. Mei, W. R. Deal, W. Yoshida, P. H. Liu, J. Uyeda, M. Barsky, L. Samoska, A. Fung, T. Gaier, and R. Lai, "Demonstration of sub-millimeter wave fundamental oscillators using 35-nm InP HEMT technology," *IEEE Microw. Wireless Compon. Lett.*, vol. 17, no. 3, pp. 223–225, Mar. 2007.

[6] W. R. Deal, X. B. Mei, V. Radisic, K. Leong, S. Sarkozy, B. Gorospe, J. Lee, P. H. Liu, W. Yoshida, J. Zhou, M. Lange, J. Uyeda, and R. Lai, "Demonstration of a 0.48 THz amplifier module using InP HEMT transistors," *IEEE Microw. Wireless Compon. Lett.*, vol. 20, no. 5, pp. 289–291, May 2010.

[7] J.-W. Shi, S.-W. Chu, M.-C. Tien, C.-K. Sun, Y.-J. Chiu, and J. E. Bowers, "Edge-coupled membrane terahertz photonic transmitters based on metal–semiconductor–metal traveling-wave photodetectors," *Appl. Phys. Lett.*, vol. 81, no. 27, pp. 5108–5110, Dec. 2002.

[8] T.-F. Kao, H.-H. Chang, L.-J. Chen, J.-Y. Lu, A.-S. Liu, Y.-C. Yu, R.-B. Wu, W.-S. Liu, J.-I. Chyi, and C.-K. Sun, "Frequency tunability of terahertz photonic transmitters," *Appl. Phys. Lett.*, vol. 88, no. 9, pp. 093501-1–093501-3, Feb. 2006.

[9] Y.-R. Huang, C.-C. Kuo, C.-M. Chiu, H.-P. Chen, T.-F. Kao, Y.-C. Chen, A.-S. Liu, R.-B. Wu, P.-C. Chiu, J.-I. Chyi, and C.-K. Sun, "Highly directed radiation pattern from a THz photonic transmitter with a two-dimensional rampart slot array antenna," *IEEE Photon. Technol. Lett.*, vol. 20, no. 12, pp. 1042–1044, Jun. 2008.

[10] J.-Y. Lu, L.-J. Chen, T.-F. Kao, H.-H. Chang, H.-W. Chen, A.-S. Liu, Y.-C. Chen, R.-B. Wu, W.-S. Liu, J.-I. Chyi, and C.-K. Sun, "Terahertz microchip for illicit drug detection," *IEEE Photon. Technol. Lett.*, vol. 18, no. 21, pp. 2254–2256, Nov. 2006.

[11] P. H. Bolívar, M. Nagel, F. Richter, M. Brucherseifer, H. Kurz, A. Bosserhoff, and R. Büttner, "Label-free THz sensing of genetic sequences: Towards "THz biochips"," *Philosoph. Trans. R. Soc. Lond. A*, vol. 362, no. 1815, pp. 323–335, Feb. 2004.

[12] J.-Y. Lu, J. Y. Lu, C. C. Kuo, C. M. Chiu, H. W. Chen, Y. J. Hwang, C. L. Pan, and C. K. Sun, "THz interferometric imaging using subwavelength plastic fiber based THz endoscopes," *Opt. Exp.*, vol. 16, no. 4, pp. 2494–2501, Feb. 2008.

[13] C.-M. Chiu, H.-W. Chen, Y.-R. Huang, Y.-J. Hwang, W.-J. Lee, H.-Y. Huang, and C.-K. Sun, "All-terahertz fiber-scanning near-field microscopy," *Opt. Lett.*, vol. 34, no. 7, pp. 1084–1086, Apr. 2009.

[14] H. Chen, T. H. Chen, T. F. Tseng, J. T. Lu, C. C. Kuo, S. C. Fu, W. J. Lee, Y. F. Tsai, Y. Y. Huang, E. Y. Chuang, Y. J. Hwang, and C. K. Sun, "High-sensitivity in vivo THz transmission imaging of early human breast cancer in a subcutaneous xenograft mouse model," *Opt. Exp.*, vol. 19, no. 22, pp. 21 552–21 562, Oct. 2011.

[15] H. Chen, W. J. Lee, H. Y. Huang, C. M. Chiu, Y. F. Tsai, T. F. Tseng, J. T. Lu, W. L. Lai, and C. K. Sun, "Performance of THz fiber-scanning near-field microscopy to diagnose breast tumors," *Opt. Exp.*, vol. 19, no. 20, pp. 19 523–19 531, Sep. 2011.

[16] R. Mendis and D. M. Mittleman, "Whispering-gallery-mode terahertz pulse propagation on a curved metallic plate," *Appl. Phys. Lett.*, vol. 97, no. 3, pp. 031106-1–031106-3, Jul. 2010.

[17] R. Mendis and D. M. Mittleman, "Comparison of the lowest-order transverse-electric (TE1) and transverse-magnetic (TEM) modes of the parallel-plate waveguide for terahertz pulse applications," *Opt. Exp.*, vol. 17, no. 17, pp. 14 839–14 850, Aug. 2009.

[18] J.-W. Shi, K.-G. Gan, Y.-J. Chiu, Y.-H. Chen, C.-K. Sun, Y.-J. Yang, and J. E. Bowers, "Metal–semiconductor–metal traveling-wave photodetectors," *IEEE Photon. Technol. Lett.*, vol. 13, no. 6, pp. 623–625, Jun. 2001.

[19] J.-W. Shi, K.-G. Gan, Y.-H. Chen, C.-K. Sun, Y.-J. Chiu, and J. E. Bowers, "Ultrahigh-power-bandwidth product and nonlinear photoconductance performances of low-temperature-grown GaAs-based metal–semiconductor–metal traveling-wave photodetectors," *IEEE Photon. Technol. Lett.*, vol. 14, no. 11, pp. 1587–1589, Nov. 2002.

[20] J.-W. Shi and C.-K. Sun, "Design and analysis of long absorption-length traveling-wave photodetectors," *J. Lightwave Technol.*, vol. 18, no. 12, pp. 2176–2187, Dec. 2000.
[21] J. Sor, Y. Qian, and T. Itoh, "A novel low-loss slow-wave CPW periodic structure for filter applications," in *IEEE MTT-S Int. Microw. Symp. Dig.*, 2001, vol. 1, pp. 307–310.
[22] Y.-R. Huang, H.-P. Chen, B.-H. Wang, S.-Y. Chen, P.-C. Chiu, J.-I. Chyi, and C.-K. Sun, "Terahertz photonic transmitters with a high-gain open-ended rampart slot array antenna," in *Proc. SPIE*, San Francisco, CA, 2010, vol. 7601, p. 760 10F-8.
[23] S.-Y. Chen and P. Hsu, "Open-ended rampart slot array antenna fed by a CPW," *IEEE Antennas Wireless Propag. Lett.*, vol. 4, no. 1, pp. 320–322, 2005.
[24] Z. G. Lu, P. Campbell, and X.-C. Zhang, "Free-space electro-optic sampling with a high-repetition-rate regenerative amplified laser," *Appl. Phys. Lett.*, vol. 71, no. 5, pp. 593–595, Aug. 1997.
[25] R. N. Simons, *Coplanar Waveguide Circuits, Components, and Systems.* New York: Wiley, 2001.
[26] I. Daubechies, "The wavelet transform, time-frequency localization and signal analysis," *IEEE Trans. Inf. Theory*, vol. 36, no. 5, pp. 961–1005, Sep. 1990.
[27] D. M. Pozar, *Microwave Engineering*, B. Zobrist, Ed. 3rd ed. Hoboken, NJ: Wiley, 2005, pp. 276–277.
[28] Y.-C. Chen, S.-Y. Chen, and P. Hsu, "A modified CPW-fed slot loop antenna with reduced cross polarization and size," *IEEE Antennas Wireless Propag. Lett.*, vol. 10, pp. 1124–1126, 2011.
[29] N. Zamdmer, Q. Hu, K. A. McIntosh, and S. Verghese, "Increase in response time of low-temperature-grown GaAs photoconductive switches at high voltage bias," *Appl. Phys. Lett.*, vol. 75, no. 15, pp. 2313–2315, Oct. 1999.
[30] J.-W. Shi, Y.-H. Chen, K.-G. Gan, Y.-J. Chiu, J. E. Bowers, M.-C. Tien, T.-M. Liu, and C.-K. Sun, "Nonlinear behaviors of low-temperature-grown GaAs-based photodetectors around 1.3-μm telecommunication wavelength," *IEEE Photon. Technol. Lett.*, vol. 16, no. 1, pp. 242–244, Jan. 2004.
[31] M.-C. Tien, H.-H. Chang, J.-Y. Lu, L.-J. Chen, S.-Y. Chen, R.-B. Wu, W.-S. Liu, J.-I. Chyi, and C.-K. Sun, "Device saturation behavior of submillimeter-wave membrane photonic transmitters," *IEEE Photon. Technol. Lett.*, vol. 16, no. 3, pp. 873–875, Mar. 2004.
[32] M. Tani, S. Matsuura, K. Sakai, and S. Nakashima, "Emission characteristics of photoconductive antennas based on low-temperature-grown GaAs and semi-insulating GaAs," *Appl. Opt.*, vol. 36, no. 30, pp. 7853–7859, Oct. 1997.